*Journal of Directed Energy*, **2**, Fall 2007, 325–346

# Aperture Effects in Aero-Optics and Beam Control

**John P. Siegenthaler* and Eric J. Jumper**

*Hessert Laboratory, Center for Flow Physics and Control, University of Notre Dame, Notre Dame, Indiana 46446-5684*

*In many beam control applications, the control is applied in separate stages through separate devices. Commonly, beam steering and tracking is performed with a flat mirror on a gimbaled mount, and in some applications this is the only form of beam control used. Wavefront correction, if present, is usually performed with a separate system and control loop. It has been known for a few years that there is an upper bound on the frequencies of disturbances that can be corrected with tip-tilt correction alone. This is caused by relations between the size of the beam aperture, the size of the variations in the air that cause aberrations in the beam, and the velocity at which the fluid variations pass through the beam (or the velocity of the beam sweeping through the variations). Variations and structures within the fluid with a length scale larger than the aperture primarily impose a deflection upon a beam. Effects on a scale smaller than the beam diameter manifest as wavefront distortions within the beam. The former can be corrected with a tip-tilt system; the latter cannot. This combined effect of aperture and beam steering correction can be regarded as a filter with a frequency-dependent gain that can be found experimentally or analytically.*

**KEYWORDS:** Beam steering, Correction bandwidths, Tilt correction, Scaling

## Nomenclature

| | |
|---|---|
| $A_p$ | length scale of aperture in Notre Dame experiments and analysis |
| $B$ | amplitude of oscillation |
| $C$ | cross-spectral density between two signals or auto-spectral density of a signal with itself |
| $D$ | diameter of aperture in Boeing SVS/Massachusetts Institute of Technology tests |
| $f$ | frequency |
| $f_d$ | dominant frequency at a location |
| $G$ | magnitude of aperture-filter frequency response |
| $g$ | generic function |
| $\mathrm{OPD}_{\mathrm{rms}}$ | root mean square of the optical path difference (OPD) over an aperture |
| $r_u$ | velocity ratio $U_2/U_1$ |
| $s$ | density ratio $\rho_2/\rho_1$ |

Received December 7, 2006; revision received May 29, 2007.
*Corresponding author; e-mail: jsiegent@nd.edu.

| | |
|---|---|
| $U_C$ | convective velocity of a flow |
| $U_{1,2}$ | sheer layer flow velocities |
| $V$ | velocity of phase screen motion |
| $\alpha_x$ | deflection angle of a beam in the $x$ direction |
| $\gamma$ | coherence function |
| $\delta_{\text{vis}}$ | vorticity thickness |
| $\Lambda$ | vortice/structure size |
| $\rho$ | density |

## 1. Introduction

When a laser beam with an otherwise planar wavefront is projected through a variable-index-of-refraction turbulent flow, its wavefront becomes aberrated. To the extent that the wavefront is aberrated across the beam's aperture, the beam's ability to create a high-intensity spot at the target in the far field is hampered.[8] An adaptive-optics (AO) system can be used to measure and then compensate for the aberrations that are to be imprinted on the beam's wavefront by imposing a conjugate wavefront figure on the beam prior to projecting it through the aberrating medium so that in a perfect case the beam emerges unaberrated.[17] In practice the conjugate is most often imposed in at least two stages. First, the aberration must be measured. Because of the linear nature of optics, the aberration that will be imposed by a beam propagating through the aberrating medium in one direction can be determined by measuring the aberration imposed by an otherwise near-planar wavefront propagated through the medium in the opposite direction. Presumably this would be some sort of return from the target. In the case of a free-space communication system, the target is cooperative and can emit a diverging beam that will arrive at the entrance pupil of the beam director as if it were a pinhole source at the target. The wavefront from this far-field return then enters the AO beam train.

One realization of the layout of the AO beam train is the Notre Dame AO system designed by Xinetics in cooperation with the Albuquerque Boeing SVS group. A schematic of the system is shown in Fig. 1. What can be noted in Fig. 1 is that the first correction element the incoming beam encounters is a tip-tilt (T/T) mirror. As implemented, this portion of the system makes use of technology that has long been available for maintaining alignment between multiple optical benches and in the present case is, in fact, used to maintain the alignment of the incoming beam into the remaining elements of the system. This schematic shows one of the critical placement considerations of the T/T mirror; the T/T mirror is reimaged on the deformable mirror (DM), which, in effect, adds an ability of the DM to tip and tilt. Some systems do use a DM or similar system for some T/T correction, but the dynamic range of such systems is often very limited in comparison to the degree of deflection that a flat mirror on gimbals can achieve.

Note also that the T/T mirror is controlled by a separate, in this case analog, stand-alone processor. The beam is focused onto a position-sensing device, which in this case is a quad cell. T/T mirrors can be made to have relatively high bandwidth so that one can presume that the remainder of the AO system need not contend with removing overall tip and tilt. In fact, almost all modern beam director systems incorporate T/T mirrors on their optical benches even when no other AO system components are present. It should be noted that we have also incorporated near-stationary correction components into our AO system for some experiments to remove mean aberration.

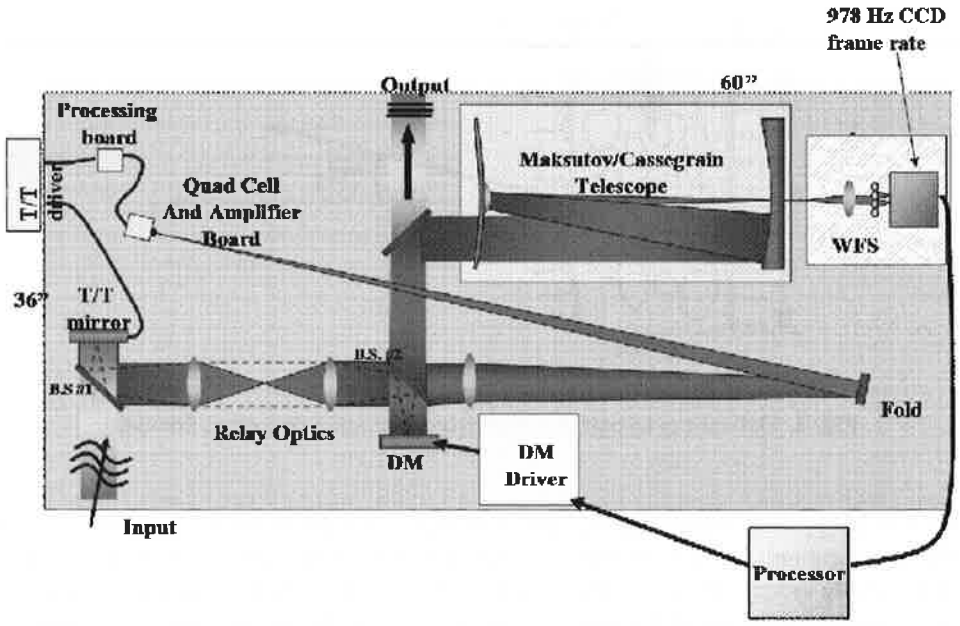


**Fig. 1.** Schematic of Notre Dame AO system cooperatively developed by Xinetics and Boeing SVS. CCD, charge-coupled device.

Because of the ubiquitous use of T/T mirrors, when we make time-resolved wavefront measurements to characterize aero-optic environments, we typically remove both tip and tilt and time-averaged mean aberration, leaving only the unsteady component over the aperture. It is important to note that the aperture itself imposes a spatial filter on the overall aberrating character of the medium. Because the aberrations are due to turbulent flow, which by definition is convecting, this spatial filter is associated with a temporal frequency. Thus, low-frequency aberrations with coherence length $\Lambda$ and a convection velocity $U_C$ will result in low-bandwidth mean tip and tilt over the aperture, which a T/T mirror will remove. Higher-frequency aberrations with a length scale smaller than the aperture do not result in mean tilt over the aperture as a whole, and so are largely unaffected by the T/T mirror. The dividing point between these two regions is that of aberrations with $\Lambda$ equal to the aperture length ($A_p$) and a frequency of $U_C/A_p$.

## 2. Aero-Optics

Optical distortions can be thought of in terms of deflection angles for isolated rays of light, or as wavefronts. A wavefront is a sheet of light with the same wavelength and phase throughout. A planar wavefront is a flat sheet of this sort and models what one might expect in a collimated laser beam of some nonzero aperture. A wavefront is a more complete expression of the optical effects of a flow, as a wavefront is composed of all the rays passing through the flow from that direction or source.

While a wavefront contains all the relevant aspects of the light and distortions to the light passing through an aberrating flow or medium, there is such a thing as having too much information. Interferometry and phase diversity can measure a wavefront in its entirely, and

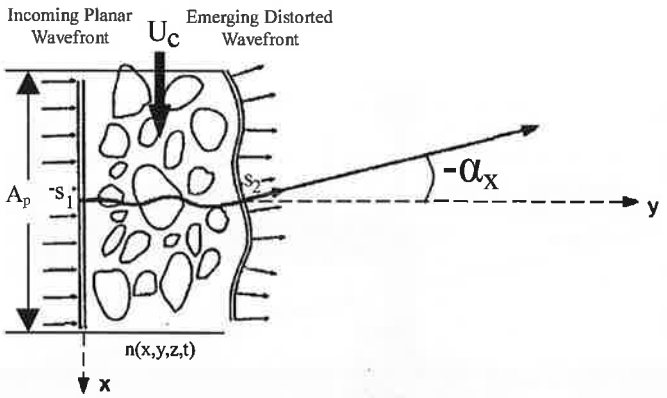


**Fig. 2.** Optical ray as part of a wavefront through a distorting flowfield.

some other types of sensors can be built with impressive spatial resolution. However, for many applications, far less information is better. For real-time applications dealing with a time-varying system, there is often a trade-off between how rapidly one can sample and process data and the amount of data one can sample. The data in this paper were acquired with a Malley probe,[5] which uses two beams that are narrow, relative to the length scale of structures in the flow, and so are deflected as rays rather than distorted as wavefronts. A detailed description of the components and reconstruction methods for optical wavefronts using a Malley probe can be found in Ref. 5.

By definition, a wavefront is a locus of points of constant phase.[10] As shown in Fig. 2, as an initially planar wavefront for a collimated laser beam propagates through a region of variable index of refraction, portions of the wavefront become advanced and retarded from the wavefront's mean position. If a plane is drawn normal to the wavefront's mean propagation direction, the beam's phase along that plane will be greater or less than the phase of the wavefront at the mean position. The phase difference over this plane is referred to as the beam's aberration. According to Huygens's principle, the wavefront can be replaced by pinhole sources along its surface, each emitting spherical waves, and the wavefront can be redrawn at some distance by connecting surfaces of constant phase from the pinhole sources.[10] This leads to the result that wavefronts propagate normal to themselves and is the basis for geometric optics. As a consequence, a ray everywhere perpendicular to the wavefront can be traced along the wavefront's propagation path as shown in Fig. 2. The angle at which the ray emerges from the aberrating medium, being normal to the emerging wavefront, will have an off-axis angle, shown as $-\alpha_x$ in Fig. 2, which is equal to the wavefront's $x$ gradient.

In the near field, optical effects are often expressed in terms of deflection angles, wavefronts, and optical path difference (OPD).

Deflection angles refer to a single ray traced through the flow. As the ray encounters variations in the medium, it deviates from its original direction of travel. After experiencing many incremental deviations, it finally emerges from the region of aberrating effects with some net deflection, seen as $-\alpha_x$ in Fig. 3.

In regions with a higher index of refraction, light travels more slowly, and from an optical standpoint, paths through such regions are effectively longer than those through regions with a lower index of refraction. The optical path length (OPL) is this effective length that the

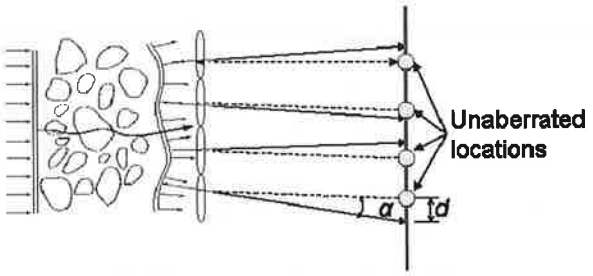


**Fig. 3.** Shack–Hartmann sensor.

light has to travel. The OPD is the mean-removed variation in OPL. It is also the conjugate of the wavefront, and the terms OPD and wavefront are often used interchangeably. Optical correction is often a matter of using a variable surface or medium to impose a wavefront that is the conjugate of the wavefront effects induced by the fluids through which the beam passes.

Beam aberrations tend to be divided into beam deflection effects and scintillation. If the aberrating structures encountered by a beam are much larger than the beam, then the beam as a whole is deflected but there is little effect in the far-field intensity patterns, and correction of this aberration is primarily a matter of beam steering. If instead of encountering large structures singly, the beam encounters numerous sources of aberration that are significantly smaller than the beam aperture of the beam, then a random scattering may occur, spreading the energy and blurring the far-field pattern. In cases between these two extremes, when the length scale of the aperture and the length scale of the aberrating structures are of the same order, then the central lobe of the unaberrated far-field pattern may be split into one or more discrete bright spots.

Hartmann was the first to realize that this fact could be used to measure the figure of wavefronts.[12] He placed an opaque, perforated plate in front of the aberrated wavefront with a photographic plate at a known distance from the perforated plate. By exposing the photographic plate first to an unaberrated beam and then to the aberrated beam, he was able to measure the off-axis displacement of beams emerging from the perforations. Knowing the distance between the plates, he could determine the angles and thus the wavefront slopes at each perforation (measurement location) and then through integration determine the wavefront's aberrated figure. Similar measurements can be made by passing small-aperture beams through the aberrating medium. A Shack–Hartmann sensor, as shown in Fig. 3, uses lenslet arrays rather than pinhole arrays, focusing the light to a point. The displacement of this point is an indicator of the average slope of the wavefront over the area of the lens.

Malley et al. were the first to recognize that when the aberrating medium is a turbulent flow, the aberrations caused by the convecting flow structures will convect as well.[13] Thus, a single beam propagated through the flow could be used to measure a continuous time series of wavefront slopes as the wavefront convects by the measurement location. The Malley principle has been used at Notre Dame to develop a series of wavefront measurement devices.[3,7,9] To the extent that the flow can be treated as slowly varying, the Taylor frozen-flow assumption can be used to compute wavefronts upstream and downstream of the measurement location, which are reasonably accurate for some distance upstream and downstream. By propagating two small-aperture, closely spaced beams aligned in the streamwise direction through the flow, both the wavefront's slope and its convection speed

can be determined:

$$\frac{\mathrm{dOPL}(t)}{\mathrm{d}x} = -\alpha_x(t). \tag{1}$$

To integrate the slope to produce a running time series of OPL($t$), the velocity is required as

$$\mathrm{OPL}(t) = \int \frac{\mathrm{dOPL}(t)}{\mathrm{d}x}\mathrm{d}x = \int \frac{\mathrm{dOPL}(t)}{\mathrm{d}x} U_C \mathrm{d}t, \tag{2}$$

where $U_C = \mathrm{d}x/\mathrm{d}t$. By knowing the distance between beams and cross correlating the beams to find the delay time between the two beams' signals, $U_C$ can be determined,[5] so that

$$\mathrm{OPL}_x(t) = \int_{t_0}^{t} -\alpha_x(\tau) U_C \mathrm{d}\tau. \tag{3}$$

From these equations and relationships, an approximation of the OPL over a portion of the flow can be reconstructed from spatially coarse data, or even a single point of measurement. An important aspect of wavefronts that becomes apparent in this form of reconstruction is the relationship between the length scale of the aberrations and the amplitude of the resulting OPD. If $\alpha_x$ were a pure sine wave, then the OPL would be

$$\mathrm{OPL}_x(t) = \int_{t_0}^{t} -B \sin(2\pi f \tau) U_C \mathrm{d}\tau = U_C \frac{B}{2\pi f} \cos[2\pi f (t - t_0)]. \tag{4}$$

By Eq. (4), the amplitude of OPLs associated with deflection data of a given amplitude will be inversely proportional to the frequency of that deflection and directly proportional to the length of the structures.

The OPL produced by Eqs. (1)–(4) can be made to any aperture width by setting the upper and lower bounds of the integral and by relating intervals in time to intervals in space by the relationship $\Delta x = U_C \Delta t$. However, the measurement technique is valid only if the frozen-flow assumption is valid, and that is true only for regions close to the points where the beam passes through the flow. As one extrapolates an OPL farther upstream or downstream from a location of measurement, the data become less valid with increasing distance from that point.

As this research was originally aimed at providing wavefront correction, it has been common practice at Notre Dame to remove T/T (beam deflection) when reconstructing these wavefronts. This is accomplished by producing a linear fit to the OPL over the indicated aperture and then subtracting that linear function from the OPL. The function that remains after this step is the OPD within the beam, ignoring any net deflection or piston applied to the wavefronts. This procedure has some interesting results that are explored later in this paper.

## 3. Motivations for Research

The end goal for much research in directed energy is the mounting of a practical, useful laser system on an aircraft. The AO research at Notre Dame is no exception to this. As an example, a practical laser-based system installed on an aircraft might involve a turret not dissimilar from the design shown in Fig. 4, having a spherical or hemispherical turret on a cylindrical base of roughly the same radius $R$. Another physical dimension of importance

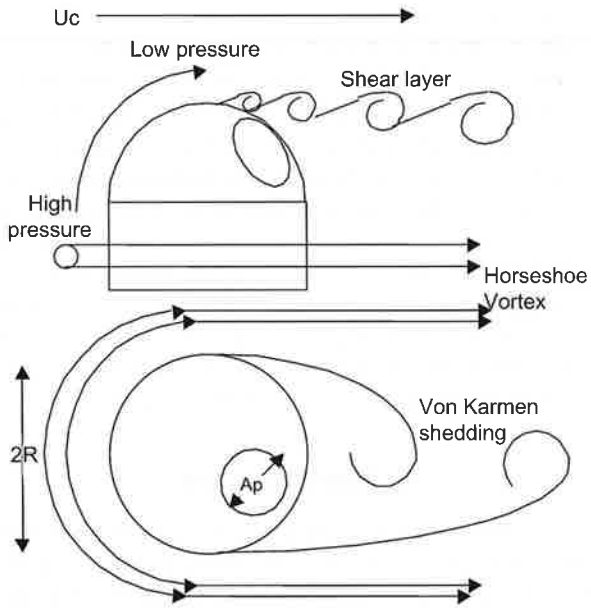


**Fig. 4.** Example turret flows.

in this is the size of the window through which a beam can be directed, as this determines $A_p$. The flow around such a turret would include a number of different types of flow and effects unique to those forms.

The mean flow over this turret would include a stagnation point at the foremost point of the turret, or at the very least an area where the flow has a lower relative speed than the airspeed of the aircraft. The flow would then accelerate over and around the turret, reaching relative speeds higher than the craft's airspeed. In the lee of the turret would be a region of separated flow.

By Bernoulli's equations, the air in the low-speed region at the fore would be of a higher pressure than that of the air the craft would be flying through. By the same principle, the air in the regions of higher speeds would have a lower pressure. In compressible or weakly compressible flow conditions, this variation in pressure will have an associated variation in density and an associated variation in index of refraction. The optical effect would be much like a large, static lens of various thicknesses encircling the turret.

The conditions for this sort of steady, laminar flow are almost never found around a physical aircraft in flight, so some time-varying components would also be seen. For the geometry in Fig. 4, a horseshoe vortex would form in front of the supporting cylinder and wrap around the sides. Von Kármán shedding will produce vortices with a frequency[6] such that $R \cdot f/U_C \approx 0.1$. These vortices will be of roughly the same length scale as the turret itself. Any form of rotational flow requires a region of low pressure within the vortex to enforce the curvature of the flow. Again, variations in pressure produce variations in density, and each vortex has an optical effect somewhat similar to a moving and evolving lens.

At points of separation, caused by the edge of a flat window in the turret for the beam to pass through, or even by the flow around a completely rounded turret, shear layers would form. The vortical structures in this flow would initially form at a relatively small size, and then grow as they progressed downstream.

It should be noted that all of these flows are very different from Kolmogorov turbulence. The energy being added to the flow through interaction with the turret is on a scale close to that of $A_p$ and often has a preferential direction. It does not have time to spread to other scales and orientations so as to reach the equilibrium conditions that are assumed for Kolmogorov turbulence. This calls into question whether the parameters normally used in AO design are applicable, as they are based on the Kolmogorov model. However, a full comparison of aero-optic and atmospheric propagation problems is a subject for a paper unto itself.

This research focuses on the aero-optic effects of shear layers. A study of shear layers can be applied to geometries other than the one shown in Fig. 4. Shear layers can and will form in many areas of separated flow, regardless of what causes the separation. Any turret or structure projecting into a flow is likely to have such a separation region, as would an optical window in a recessed cavity instead of a projecting turret.

## 4. Shear Layers

Shear layers (Fig. 5), also known as mixing layers, occur at the boundary between two parallel flows of different fluids, or even the same fluid moving at different velocities. The transfer of momentum in the vicinity of the boundary causes this boundary region to grow in size as it convects downstream. Kelvin–Helmholtz instability produces ripples in the boundary along its span that also grow and contribute to the growth of the layer region. These perturbations eventually roll up into vortical structures that grow, pair, and merge as the shear layer grows.[6]

When there is a large difference in relative velocity between the two flows, the low-pressure well found in the center of these structures, also known as rollers, can be quite pronounced.[4] This drop in pressure is accompanied by a drop in density, with its concomitant change in index of refraction. This makes these structures of interest from an optical standpoint. While many elements in a compressible flow of this sort can produce optical distortions, the low-pressure wells associated with these rollers are likely to be the most significant contributor in that regard. This is also another significant difference between aero-optics and atmospheric propagation, as temperature variations are normally assumed to be the primary source of aberrations in the atmospheric case.

Shear layers grow linearly in thickness with distance from their starting point. There are multiple definitions for the thickness of a shear layer, such as momentum thickness and vorticity thickness, and the growth rate of the shear layer is less well understood for compressible flows than for incompressible and weakly compressible shear layers. In

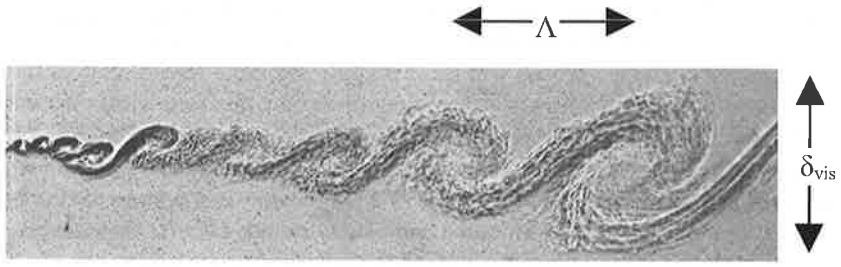


**Fig. 5.** Classic shear layer.[11]

these experiments, the primary method for estimating the layer thickness was by visual observation of the vortical structures in the flow. This vorticity thickness[16] $\delta_{\text{vis}}$ can be estimated from the following empirical relation:

$$\frac{\mathrm{d}\delta_{\text{vis}}}{\mathrm{d}x} \approx 0.17\frac{(1-r_u)(1+\sqrt{s})}{1+r_u\sqrt{s}}, \tag{5}$$

where $r_u$ is the velocity ratio $U_2/U_1$ and $s$ is the density ratio $\rho_2/\rho_1$ of the two flows making up the shear layer.

For this optical study, the dimension in the layer of primary interest is not the thickness, but the spacing between rollers ($\Lambda$). This coherence length is related to $\delta_{\text{vis}}$ by yet another empirical constant. The literature reports that this ratio of $\Lambda/\delta_{\text{vis}}$ varies from 1.5 (Ref. 1) to 2 (Ref. 2). In observing a flow passing a point of measurement, the average length of a repeating structure can be found by the relationship

$$\Lambda = U_C/f_d, \tag{6}$$

where $f_d$ is the frequency or average frequency at which the structure is seen to pass by the point of measurement. In these studies, $f_d$ was taken to be the frequency with the highest magnitude on a power spectral density (PSD) of beam deflection. However, there are other methods to this, such as weighted averaging.

## 5. Experimental Setup

The experiments for this study were performed using the Notre Dame Weakly-Compressible Shear Layer (WCSL) facility, shown in Fig. 6, located in Notre Dame's Hessert Laboratory for Aerospace Research.

The WCSL facility consists of an inlet nozzle and test section mated with one of Notre Dame's three transonic in-draft, wind-tunnel diffusers. The diffuser section is attached to a large, gated plenum. The plenum is, in turn, connected to three Allis Chalmer 3,310 cubic feet per minute (CFM) vacuum pumps through a sonic throat to prevent unsteady effects from propagating upstream from the pumps. Depending on the gate–valve arrangements, each of these pumps can be used to power separate diffusers, or they can be used in combination to power a single diffuser.

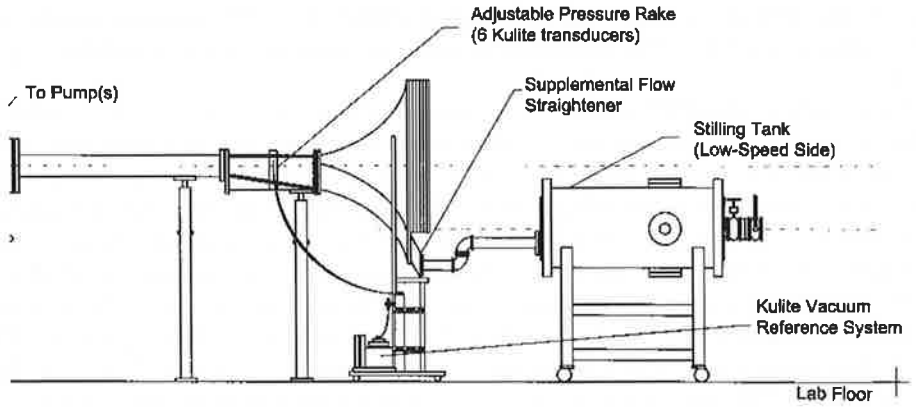


**Fig. 6.** Notre Dame WCSL facility.

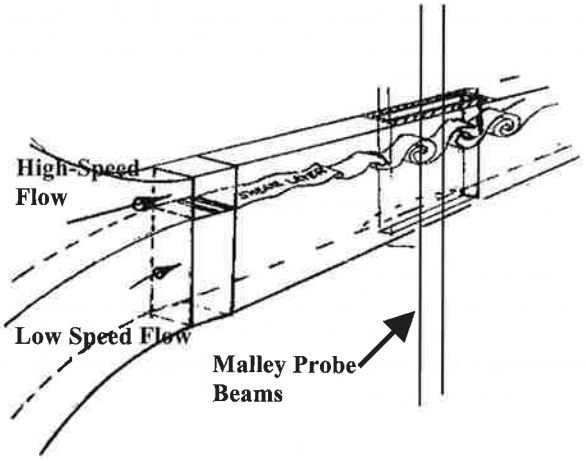


**Fig. 7.** Malley probe positioning.

Because it is an in-draft tunnel, the feeding source is the room total pressure and temperature. The test section is fed from a 104-to-1 inlet nozzle directly from room total pressure on the high-speed side. On the low-speed side, room-total-pressure air is first passed through a settling tank with a "quiet valve" consisting of a bundle of pipes that the flow is forced to pass through at high speed. This produces a loss in total pressure, while keeping the total temperature the same as that of the room air drawn into the high-speed side.

In this set of experiments, a Malley probe[5] was used to assess the optical aberrations. In the present case, the Malley probe's two laser beams were directed through the test section from below, as shown in Fig. 7. All data were filtered to prevent aliasing and to remove low-frequency effects of tunnel vibrations.

## 6. Physical Results

The data presented here are for the shear layer running with Mach number values of 0.88 and 0.06 for the high-speed and low-speed flows, respectively. At the pressure and temperature conditions in the test section, this translates to velocities of approximately 285 and 22 m/s, with a convection velocity for the shear layer between them of 153 m/s. By Eq. (5), this indicates a $\delta_{vis}$ growth rate of approximately 0.27. The predicted growth rate for $\Lambda$ ranges from 0.4 to 0.54, depending on which recommendation for this relationship is used.[1,2]

Figure 8 shows the PSD for a number of streamwise positions in an example shear layer. There is an identifiable peak frequency, which becomes lower as the measurement location moves farther downstream. Owing to variations in the flow with each rolling structure that goes by, this peak is part of a broadband set of frequencies rather than one isolated frequency. However, it is still possible to identify a central or average frequency in this manner.

Figure 9 shows the peak frequency of optical disturbances in the shear layer as a function of position downstream from the origin of the shear layer. Figure 10 shows the structure length estimated from the frequencies in Fig. 9 and the convection velocity by Eq. (6). The trend does appear linear, which is consistent with the expected behavior of this flow. The line in Fig. 10 represents a value of 2 for $\Lambda/\delta_{vis}$, which is the maximum value for this ratio found in the literature referenced earlier.[2]

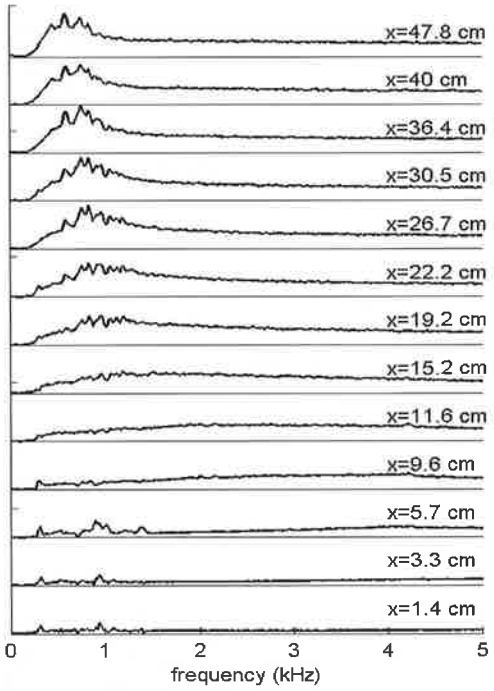


**Fig. 8.** Beam deflection power density spectra for various streamwise positions.

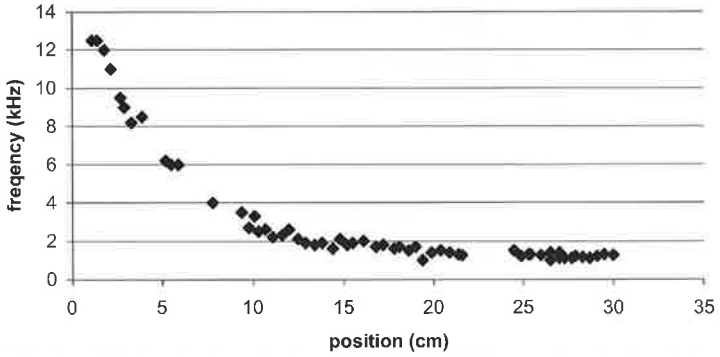


**Fig. 9.** Peak deflection frequencies.

Figure 11 shows the time-averaged root mean square OPD with T/T removed ($OPD_{rms}$) at various streamwise positions. There are five separate curves in this figure, but all of them are based on the same data recorded at those positions. The difference in the curves is the size to which the aperture was set in reconstructing the OPD from the recorded beam deflections. An aperture of 300 cm can effectively be considered an infinite aperture, and for that aperture size, $OPD_{rms}$ grows almost linearly with position. From Eq. (4), one would expect the amplitude to grow proportionately with $1/f$. From Eq. (6), $1/f = \Lambda/U_C$, and from the nature of shear layers, $\Lambda$ is a linear function of position. Thus, it is to be expected that the average magnitude of the optical disturbances would grow linearly with position.

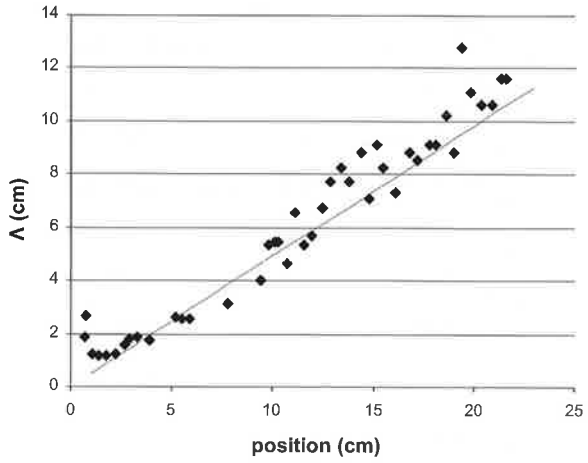


**Fig. 10.** Characteristic Λ and growth rate.

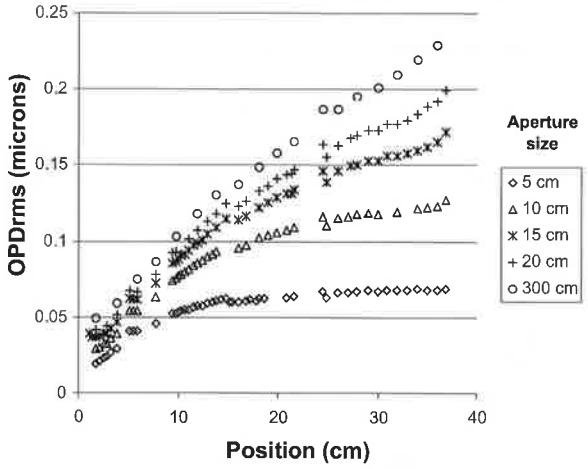


**Fig. 11.** Apertured OPD.

However, applying a smaller aperture to the data reduces the magnitude of the $OPD_{rms}$ seen within that aperture. Additionally, the shape of the curves produced changes from something close to a straight line to a curve of decreasing slope that levels off at some point. After observing this effect in the reconstructed data, an exploration of the reasons behind this was undertaken.

## 7. Aperture Effects

Figure 12 shows two wavefronts, both aberrated into the form of a sine wave. These two simulated wavefronts have the same amplitude over the same length of aperture but differ in Λ relative to that aperture length. In Fig. 12a, the period of the wave is a bit longer than the aperture. A linear fit to this wavefront over the aperture has a significant slope, which by Huygens's principle indicates a significant degree of net tilt and associated beam deflection.

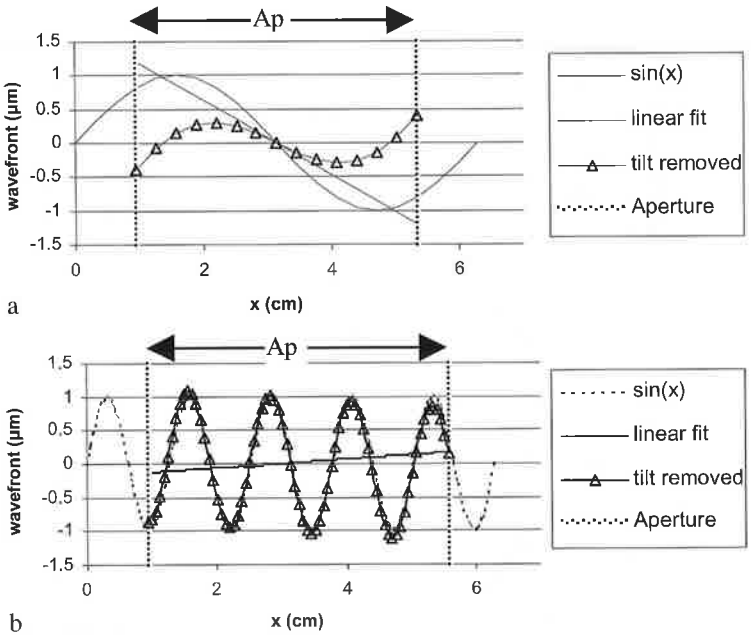


**Fig. 12.** Examples of the spatial filter effect produced by an aperture and T/T removal.

Removing this tilt to place the beam on target also reduces the amplitude of the variations in the wavefront, in this case by more than 50%. Figure 12b shows the effects of T/T removal when the spatial scale of the distortions is smaller than the aperture. In that case, there is very little net tilt and tilt removal has little effect on the magnitude of the aberration.

The finite aperture of a physical beam acts as a spatial filter, separating the distortions caused by larger-scale structures from those caused by smaller-scale structures. If $A_p/\Lambda \ll 1$, then T/T deflection becomes the only significant effect of distortions on that length scale. This would seem to indicate that the most severe wavefront distortions come from distorting structures in the flow that are smaller than the aperture. However, there is a countervailing effect seen in the wavefront reconstruction algorithms and formulas that produces OPD variations of greater amplitude for aberrations of the largest length scales. This is addressed in Eq. (4) and the associated text.

Figure 13 was generated by using a pure sine function of extended coherence length as the beam deflection $\alpha$. Each point is the time-averaged $\text{OPD}_{\text{rms}}$ for a fixed period of $\alpha$ and a fixed $A_p$. Each set of points shares a common value for $A_p$ while $\Lambda$ varies. For an infinite aperture, the average $\text{OPD}_{\text{rms}}$ grows linearly with $\Lambda$. This is to be expected from Eq. (4) and the relationship $f = U_C/\Lambda$. For a finite aperture, this is true only for $\Lambda < A_p$. For $\Lambda > A_p$, $\text{OPD}_{\text{rms}}$ tapers off asymptotically as $\Lambda$ increases. The spatial filter of the aperture, combined with the removal of T/T by a tracking system of some sort, filters out the longer wavelengths of wavefront aberration.

The results in Fig. 13 show a similarity in the curves traced for different values of $A_p$, with both the maximum value for $\text{OPD}_{\text{rms}}$ and the value of $\Lambda$ at which that maximum is seen having a linear relationship with $A_p$. Both OPD and structure size are in units of length, as is the aperture, and so it makes sense to nondimensionalize those values by $A_p$. The result

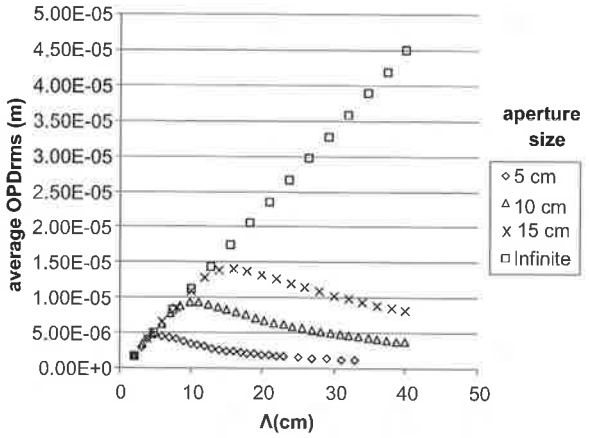


**Fig. 13.** Results for simulated $\alpha = \sin(\omega t)$.

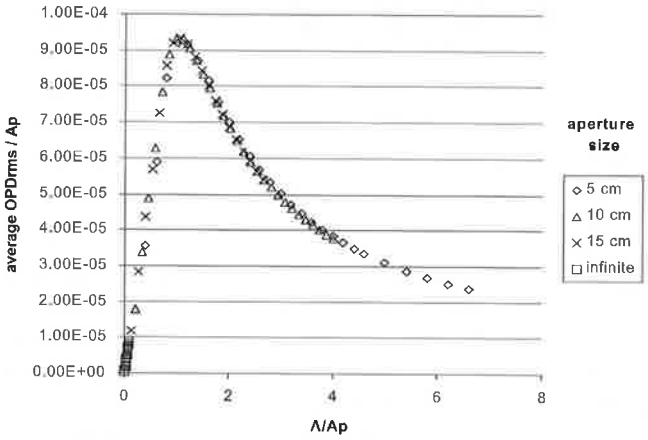


**Fig. 14.** Nondimensionalized results for $\alpha = \sin(2\pi f t)$.

of this, seen in Fig. 14, is the collapse of all the curves onto one curve. For shear layers, in which $\Lambda = x \cdot \mathrm{d}\delta/\mathrm{d}x$ and $\mathrm{d}\delta/\mathrm{d}x$ is constant, this scaling and nondimensionalization should also apply to $x/A_p$.

This result is promising, as scaling laws are valuable tools in applying laboratory results to field applications, but flows that produce optical distortions in the form of a perfect sine wave are hard to come by in the physical world.

This filter effect can also be found and expressed analytically. For a wavefront or other input of the form $g(x, t)$, $\mathrm{OPD}_{\mathrm{rms}}$, as a function of time over an aperture with T/T removal, will be

$$\mathrm{OPD}_{\mathrm{rms}}(A_p, t) = \sqrt{\int_0^{Ap} \{g(x, t) - [A(t) + xB(t)]\}^2 \mathrm{d}x}, \tag{7}$$

where $A$ and $B$ in are the coefficients of a linear fit to the overall tilt and piston present in $g(x, t)$. It just so happens that finding values for $A$ and $B$ to minimize the function inside

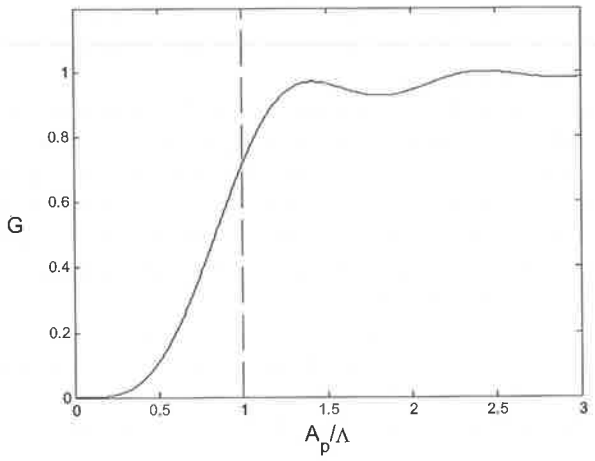


**Fig. 15.** Spatial filter normalized frequency response.

the square root in Eq. (7) is the basis for performing such a linear fit, which explains why T/T removal tends to reduce the magnitude of aberrations.

If $g(x, t)$ is set to a sine function,

$$g(x,t) = \sin\left[2\pi f\left(t - \frac{x}{U_C}\right)\right] \tag{8}$$

and the resulting $\mathrm{OPD}_{\mathrm{rms}}$ is averaged over time, then that average can be compared to the $\mathrm{OPD}_{\mathrm{rms}}$ for an infinite aperture with no T/T removal. This ratio can be considered the gain of the spatial filter for that length in the distorting structures:

$$G(A_p) = \frac{\mathrm{OPD}_{\mathrm{rms}}(A_p)}{\mathrm{OPD}_{\mathrm{rms}}(A_p = \infty)}. \tag{9}$$

Figure 15 shows the frequency response of this spatial filter in terms of a nondimensional frequency, $A_p/\Lambda = f^* A_p/U_C$. As can be seen in the figure, this is a high-pass filter, screening out aberrations with a length scale larger than the aperture. This filter gain can be found analytically from Eq. (7) for a sine signal given in Eq. (8). The use of a sine wave approximation was prompted by the results shown in Sec. 6, which indicate that shear layers tend to have a dominant frequency or frequency range. Using a pure sine wave for this derivation makes a rule-of-thumb frequency analysis possible, which can then be checked against results for more complicated wavefront forms. The gain function based on this approximation has the form

$$G(A_p/\Lambda) = \frac{-3 - \pi^2(A_p/\Lambda)^2 + \pi^4(A_p/\Lambda)^4 + \left[3 - 2\pi^2(A_p/\Lambda)^2\right]\cos^2[\pi(A_p/\Lambda)] + 6\pi(A_p/\Lambda)\sin[\pi(A_p/\Lambda)]\cos[\pi(A_p/\Lambda)]}{\pi^4(A_p/\lambda)^4}. \tag{10}$$

This filtration does not apply only to shear layers. It can be applied to any system in which a relationship between the length scale of the aberrations and the length scale of the

aperture can be determined. This includes cases expressed in terms of frequency, by the relationship $f = U_C/\Lambda$ from Eq. (6), provided that the velocity of the aperture or beam relative to the atmosphere is known.

As a practical application, this has significance for the engineering of T/T removal systems. The bandwidth that is capable of contributing to effective correction for this system corresponds to the frequencies removed by this filter function. Looking at Fig. 15, the half-power point on this curve occurs at $A_p/\Lambda \cong 0.85$. However, for rule-of-thumb purposes, a value of $A_p/\Lambda = 1$ may be more convenient. When applying this to experimental data, one should either nondimensionalize the coherence length or related property by $1/A_p$ or scale the nondimensional frequency of $G$ by $U_C/A_p$.

The scaling law is especially applicable to flows with a linearly growing self-similar form but should be applicable to comparison of different aperture sizes through the same region of a flow, regardless of the form of that flow.

It is left now to examine some actual optical data to see whether this does apply.

## 8. Applied Aperture Filtration and Scaling

Figure 16 shows the same $OPD_{rms}$ (T/T removed) for different aperture sizes as was shown in Fig. 11. With a consideration of the filter effects of the aperture and T/T correction, it is now understandable why the average OPD observed through a smaller aperture is reduced. Additionally, from the growth rate for the shear layer shown in Fig. 10, $\Lambda$ reaches 5 cm in length at a position somewhere around 11 cm, and in Fig. 16, the curve made up of $OPD_{rms}$ values generated with a 5-cm aperture begins to level off at about that point.

From the results shown in Fig. 14 for the sine wave test and model, one might expect the curves to fall off at downstream positions where the characteristic structure length seen in Fig. 10 is larger than the aperture. However, as can be seen in the power density spectra in Fig. 8, the data include high-frequency deflections as well as the lower frequencies associated with the pressure wells in the rollers. This may be caused by smaller irregularities and vortices that roll up into the larger structures, as well as the boundary layer forming along the upper surface of the test section in the high-speed flow. The spatial filter of the

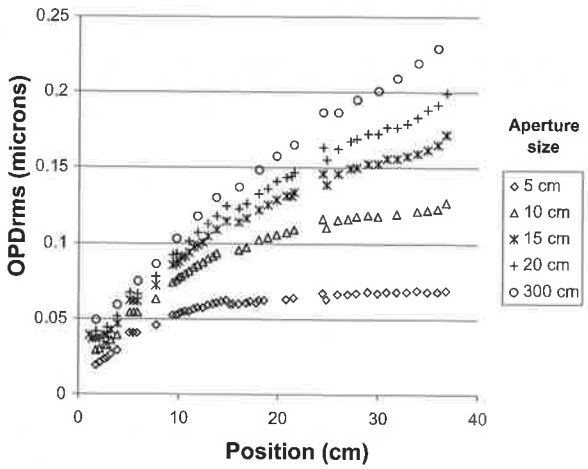


**Fig. 16.** Apertured OPD.

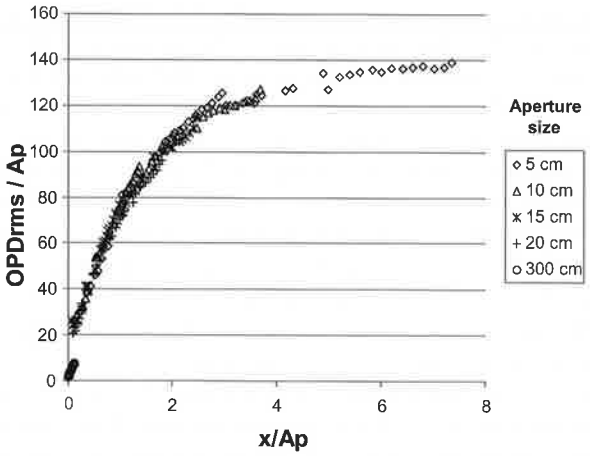


**Fig. 17.** Nondimensionalized OPD.

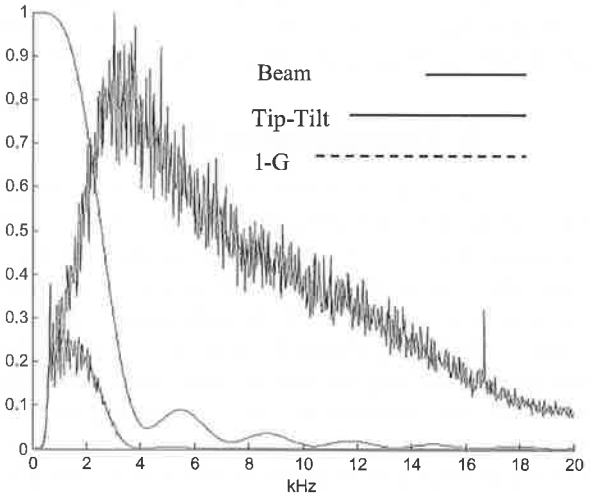


**Fig. 18.** T/T power spectrum and inverse filter.

aperture does not remove these smaller scale optical distortions, and the turbulent boundary layer grows with position downstream.

Figure 17 shows that despite these differences, the same practice of nondimensionalization shown in Fig. 14 applies to the experimental data. That the scaling law holds true for the experimental results indirectly suggests that the filter function shown in Fig. 15 and Eq. (10) also holds true, but a more direct demonstration can be made. There are difficulties in generating a PSD function for apertured OPDs from Malley probe data, as there are few points in the aperture to work with. However, it is possible to generate an apertured OPD for each time step of the recorded data, record the slope of the tilt removed, and generate a PSD of that tilt. If the T/T removal does indeed filter out frequencies from the OPD, then the dominant frequencies of the tilt should be the ones removed by that filter.

Figure 18 shows the PSD of beam deflection at a position of 9.4 cm, normalized to a maximum value of 1. Frequencies below 500 Hz have been filtered out to remove tunnel

vibration from the data. This figure also shows the T/T PSD for a 5-cm aperture to the same vertical scale. The third line on this figure is the reciprocal of the filter gain, defined here as $1 - G$. Where the function $G$ [Eqs. (9) and (10)] indicates which frequencies of aberration pass through the system without attenuation, the function $1 - G$ should then correspond to those frequencies that are removed by the filter of the aperture with T/T correction. This function has been scaled along the frequency axis to reflect the flow conditions. With $U_C = 153$ m/s and a 5-cm aperture, the rule-of-thumb cutoff frequency is $U_C/A_p = (153 \text{ m/s})/(0.05 \text{ m}) \approx 3$ kHz. The exact shape of the T/T PSD does not and could not be expected to exactly match $1 - G$, since the signal to be filtered does not have a uniform frequency distribution; however, the T/T PSD does look much like the product of the beam deflection PSD and $1 - G$. From this, it is also clear that disturbances of a frequency above 3–4 kHz are ignored by the T/T correction being applied.

Alternatively, the scaling function inherent in this filter effect can be used to compare the effects of different sized apertures looking through the same flow. Figures 19 and 20 show T/T spectra for the same location in Fig. 18, but for different sizes of aperture. Figure 19 is plotted against the actual frequencies, and it can be seen that increasing the size of the aperture lowers the cutoff frequency of the aperture filter. In Fig. 20, the frequencies for each spectrum have been nondimensionalized by $A_p/U_C$, and the resulting spectra are laid on top of each other, as well as fitting neatly onto the reciprocal gain $(1 - G)$.

## 9. Corroborating Results

These observations of the aperture filter effect were observed at Notre Dame in the study of shear layers. The scaling effect presented above works, in part, because a shear layer has a self-similar structure that grows linearly with distance downstream, as indicated in Eq. (5). However, this effect can be observed and applied to a wider range of flows.

Boeing SVS conducted a series of tests at the Advanced Concepts Laboratory of the Massachusetts Institute of Technology/Lincoln Laboratory in Lexington, MA.[14,15] These tests were intended to model tracking through an atmosphere rather than through a near-field flow. The atmosphere was simulated by a series of moving phase screens. From one direction, an image of a point source of light was directed through the screens to a tracking sensor and processor. In the other direction, a laser was directed along the same beam path to a scoring sensor and processor. The setup for this test is depicted in Fig. 21.

The effectiveness of tracking algorithms was evaluated by taking the output the tracking processor produced in response to the incoming point source and comparing it to the measured deflection of the outgoing laser beam. This was done with a coherence function defined as

$$\gamma^2_{x-\mathrm{tr}\,x-\mathrm{sc}}(f) = \frac{|C_{x-\mathrm{tr}\,x-\mathrm{sc}}(f)|^2}{C_{xx-\mathrm{tr}}(f)C_{xx-\mathrm{sc}}(f)}. \tag{10}$$

In Eq. (11), $C_{x-\mathrm{tr}\,x-\mathrm{sc}}(f)$ is the cross-spectral density between the beam and the tracking output, $C_{xx-\mathrm{tr}}(f)$ is the auto-spectral density of the tracking output, and $C_{xx-\mathrm{sc}}(f)$ is the auto-spectral density of the beam deflection as measured by the scoring sensor. Both signals are indicators of T/T, one for the beam deflection imposed by the phase screens and one for the mirror or other device intended to correct this aberration. A value of one for this function indicates that the tracking signal follows the beam deflection for disturbances of that frequency and thus would be able to direct a tracking or beam steering system in such a way as to correct for those beam deflections. Values of less than one

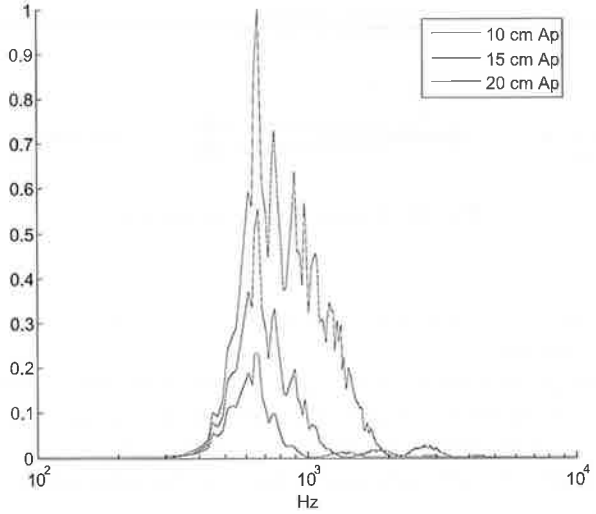


**Fig. 19.** T/T PSD for various $A_p$ values.

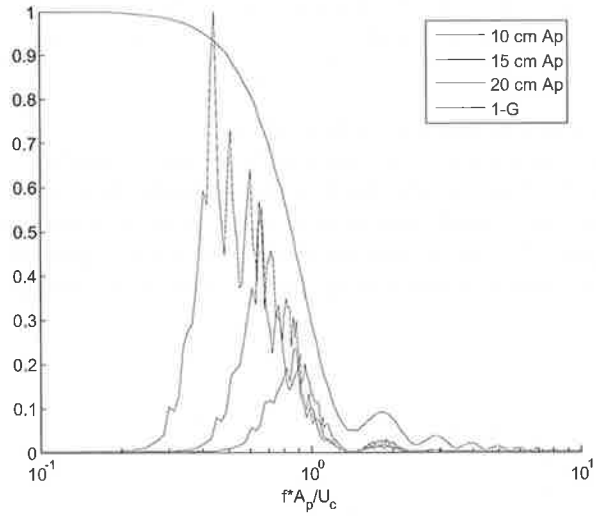


**Fig. 20.** T/T PSD with frequency scaling.

indicate less than perfect tracking, while values near zero indicate that the two signals are effectively random with respect to each other. This is similar to the Notre Dame practice of recording the T/T removed with each time step in the postprocessing reconstruction of OPD.

In these tests, it was discovered that there exists an upper limit to the frequency of disturbances that the system could track and that this frequency limit corresponded to the velocity $V$ at which the phase screens were being moved, divided by the diameter $D$ of the aperture of the system. The coherence function $\gamma$ indicates how well the tracking signal follows the induced beam deflection, and in this respect it is a counterpart to the reciprocal

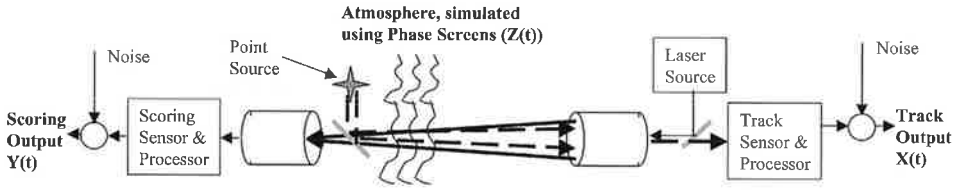


**Fig. 21.** Boeing SVS tracking test.

gain function $(1 - G)$, which indicates which frequencies of aberration are removed by T/T correction over an aperture.

To properly compare with these results, a gain function different from the one in Eq. (10) should be used. That equation is based on a one-dimensional aperture. The experiment shown in Fig. 21 had a two-dimensional circular aperture. The effective gain function for such an aperture with T/T correction can be found in the same manner as was done for Eq. (10), producing

$$G_{2D}(A_p/\lambda) = \frac{\left\{\begin{array}{l}\pi^4(A_p/\Lambda)^4 - 16\pi^2(A_p/\Lambda)^2 J_0[\pi(A_p/\Lambda)]^2 - 64J_1[\pi(A_p/\Lambda)]^2 \\ +64\pi(A_p/\Lambda)J_0[\pi(A_p/\Lambda)]J_1[\pi(A_p/\Lambda)] - 4\pi^2(A_p/\Lambda)^2 J_1[\pi(A_p/\Lambda)]^2\end{array}\right\}}{\pi^4(A_p/\Lambda)^4}, \quad (11)$$

where $J_0$ and $J_1$ are Bessel functions of the first kind.

Figure 22 shows the results of two separate tests, one in which $V/D = 1.54$ Hz and another in which $V/D = 0.38$ Hz. Both of these results have been scaled by $D/V$ along the frequency axis, which puts them in terms of the nondimensional frequency in which the filter gain $G_{2D}$ and its reciprocal were originally expressed. The two results lie on top of each other with this scaling and lie close to the unscaled reciprocal gain as well.

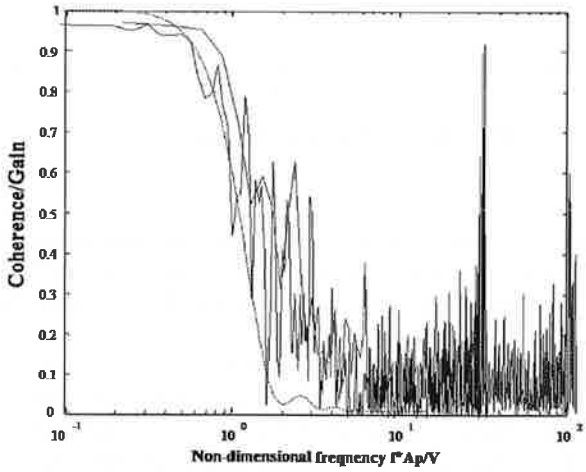


**Fig. 22.** Frequency-scaled Boeing SVS results.

## 10. Conclusion

This paper explored the effects of a spatial filter in the form of an aperture with T/T correction. With a known convection velocity, this filter can be expressed in terms of frequency rather than length scales. Length and frequency scales of the Fried parameter and Greenwood frequency exist and are used in scaling experiments and design of AO systems, but those parameters are based on Kolmogorov models of atmospheric turbulence. This work represents an approach that can be used for the types of flows commonly found in aero-optic conditions.

The existence and effects of this phenomenon must be taken into account when using scale models or comparing systems of differing sizes. This filter function also has a significant impact on the design of control system for optical correction. The cutoff frequency of $U_C / A_p$ provides a guide to the bandwidth requirements for T/T correction. Additionally, this guide can be used to avoid incurring costs for added bandwidth that would not provide significant improvement in system performance. In fact, going beyond this limit might degrade the system's signal-to-noise ratio as it attempts to cope with inputs it cannot affect.[15]

## 11. Acknowledgments

These efforts were sponsored by the Air Force Office of Scientific Research, Air Force Material Command, U.S. Air Force, under Grant F49620-03-1-0019. The U.S. Government is authorized to reproduce and distribute reprints for governmental purposes notwithstanding any copyright notation thereon.

## References

[1]Brown, G.L., and A. Roshko, J. Fluid Mech. **64**(4), 775 (1974).

[2]Dimotakis, P.E., AIAA J. **24**(11), 1791 (1986).

[3]Fitzgerald, E.J., and E.J. Jumper, Opt. Eng. **39**(12), 3285 (2000).

[4]Fitzgerald, E.J., and E.J. Jumper, J. Fluid Mech. **512**, 153 (2004).

[5]Gordeyev, S., E.J. Jumper, T. Ng, and A. Cain, "Aero-Optical Characteristics of Compressible, Subsonic Turbulent Boundary Layer," AIAA Paper 2002-3606, June 2003.

[6]Ho, C.-M., and P. Huerre, Annu. Rev. Fluid Mech. **16**, 365 (1984).

[7]Hugo, R., and E. Jumper, Appl. Opt. **35**(22), 4436 (1996).

[8]Jumper, E., and E. Fitzgerald, Progr. Aerospace Sci. **37**, 299 (2001).

[9]Jumper, E.J., and R.J. Hugo, AIAA J. **33**(11), 2151 (1995).

[10]Klein, M., *Optics*, Wiley, New York (1970).

[11]Konrad, J.H., "An Experimental Investigation of Mixing in Two-Dimensional Turbulent Shear Flows with Application to Diffusion-Limited Chemical Reactions," Ph.D. Thesis, California Institute of Technology, 1976.

[12]Malacara, D., *Optical Shop Testing*, Wiley, New York (1978).

[13]Malley, M., G.W. Sutton, and N. Kincheloe, Appl. Opt. **31**, 4440 (1992).

[14]Merritt, P., S. Peterson, R. Telgarsky, D. Brunson, R. Pringle, and S. O'Keefe, "Performance of Tracking Algorithms under Airborne Turbulence," SPIE Laser Weapons Technology Symposium, AeroSense, Orlando, FL, April 2001.

[15]Merritt, P., S. Peterson, R. Telgarsky, D. Brunson, R. Pringle, and S. O'Keefe, "Limitation on the Bandwidth of Tracking through the Atmosphere," SPIE Laser Weapons Technology Symposium, AeroSense, Orlando, FL, April 2002.

[16]Papamoschou, D., and A. Roshko, J. Fluid Mech. **197**, 453 (1988).

[17]Tyson, R.K., *Principles of Adaptive Optics*, Academic Press, San Diego, CA (1991).

## The Authors

**Dr. Eric Jumper** holds a Ph.D. in fluid dynamics and laser physics from the Air Force Institute of Technology and is a professor in the Department of Aerospace and Mechanical

Engineering at the University of Notre Dame. During more than 20 years in the Air Force, he served as a professor at AFIT, receiving the General Bernard A. Schriever Award for Research, before becoming the chief of the Laser Devices Division at Kirtland AFB. In his 17 years at Notre Dame, he has presided over the creation of an aero-optics research group, producing 10 journal articles on the subject and dozens of proceeding papers in this field. He was inducted as an AIAA fellow in 2003.

**Mr. John Siegenthaler** holds an M.S. in electrical engineering from Colorado University at Boulder, with an emphasis on controls. After a couple of years working for Honeywell in maintenance and improvement of large satellite tracking antennas, he returned to graduate school at the University of Notre Dame. He is currently finishing his Ph.D. in aerospace engineering, with an emphasis on aero-optical effects.